Available online at www.sciencedirect.com

ScienceDirect

Proceedings of the Combustion Institute 37 (2019) 373–379

Proceedings of the Combustion Institute

www.elsevier.com/locate/proci

Experimental and computational studies of the kinetics of the reaction of hydrogen atoms with carbon disulfide

Katherine E. Kerr[1], Yide Gao[2], Paul Marshall*

Department of Chemistry and Center for Advanced Scientific Computing and Modeling, University of North Texas, 1155 Union Circle #305070, Denton, TX 76203-5017, USA

Received 1 December 2017; accepted 12 June 2018
Available online 7 July 2018

Abstract

Pulsed laser photolysis at 193 nm of NH_3/CS_2 mixtures in an Ar bath gas combined with resonance fluorescence detection of atomic H yielded the rate constant for $H + CS_2$ over 295–490 K. The reaction was found to be pressure dependent and in the fall-off region or near the low pressure limit. Fitting to the Troe formalism yielded $k_0 = 7.5 \times 10^{-24}$ $(T/300\,K)^{-14.76}$ $\exp(-5180\,K/T)$ cm^6 molecule^{-2} s^{-1} over 295–490 K. At 490 K equilibration of adduct formation was observed which yielded a H-SCS bond dissociation enthalpy of 73 ± 10 kJ mol^{-1}. These observations are consistent with W1 results for the potential energy surface and comparison suggests HSCS is the major addition product. Transition state theory yields an estimate for the high-pressure limit of addition over 290–300 K of 1.3×10^{-9} $\exp(-7.2\,kJ\ mol^{-1}/RT)$ cm^3 molecule^{-1} s^{-1}. Uncertainties are discussed in the text.

Keywords: Carbon disulfide; Falloff region; Thermochemistry; Addition kinetics; Claus process

1. Introduction

The Claus process, where hydrogen sulfide and sulfur dioxide disproportionate to yield elemental sulfur, is a central step in the removal of sulfur from hydrocarbon fuels [1,2]. Undesirable by-products include carbon disulfide (CS_2) and carbonyl sulfide. In order to improve our understanding of the mechanistic details of the Claus chemistry, we have investigated the reaction

$$H + CS_2 \rightarrow \text{products} \quad (1)$$

Woiki and Roth [3] made shock tube measurements on the pathway leading to SH + CS at 1170–1830 K, and this reaction has been incorporated into a recent mechanism for CS_2 flames [4]. Carbon disulfide has been employed as a carbon source in diamond deposition [5] and reaction (1) was a potential interference in the use of CS_2 as an S-atom precursor in our laboratory studies of the $S + H_2$ reaction [6]. Because the abstraction channel is endothermic by 87 kJ mol^{-1}, it will be slow in Claus reactors operating at around 400–600 K. Here, we investigate temperatures up to ca. 500 K that have

* Corresponding author.
E-mail address: paul.marshall@unt.edu (P. Marshall).
[1] Present address: Wentworth Institute of Technology, 550 Huntington Avenue, Boston, MA 02115, USA.
[2] Present address: PPG Industries, 3333 North Interstate 35, Gainesville, TX 76240, USA.

https://doi.org/10.1016/j.proci.2018.06.091
1540-7489

not been explored previously and find evidence for a new, addition pathway. With the observation of CS_2 in comets [7], this channel might also have a role in astrochemistry. Studies of H/CS_2 interactions may also be compared to the valence isoelectronic $OH + CO/H + CO_2$ system, central to CO oxidation and heat release in combustion and where a stable HOCO intermediate was invoked to explain the unusual temperature dependence of the $OH + CO$ reaction [8]. Detailed computational studies on the $OH + CO$ system confirm formation of an HOCO adduct (and that HCO_2 is less stable), which dissociates exothermically over a barrier to $H + CO_2$ [9]. As we indicate below, similar species arise in the analogous sulfur system but differences in their thermochemistry change the ordering of relative stability. In particular, HSCS is observable as a product of $H + CS_2$ via the pressure-dependence of the measured kinetics.

2. Experimental method

Details of our apparatus for laser flash photolysis experiments with time-resolved resonance fluorescence detection of atomic hydrogen, including with other sulfur-containing species, have been provided previously [10–14] and so the method is outlined here. Inside a heated stainless steel reaction cell, H atoms are created by pulsed photolysis of a precursor at 193 nm, ammonia (NH_3) in this case, and then react with a large excess of CS_2 which is therefore effectively at constant concentration. The time scale is short compared to the time for diffusion to the reactor surfaces so the experiments are largely separated from heterogeneous processes. Resonance fluorescence from the H atoms is excited by a microwave-powered flow lamp at Lyman α, 122 nm. The photon-counting signal I_f observed with a solar-blind photomultiplier tube, and accumulated over typically several hundred pulses repeated at ca. 1 Hz in a slowly flowing mixture, is proportional to [H], plus a constant background from scattered light. NH_3 and CS_2 were purified by freeze-pump-thaw cycles with liquid nitrogen and dilutions in a large excess of argon (Ar) were prepared manometrically. Mole fractions in the mixtures, the measured flow rates of the mixtures and further pure Ar into the reactor, the pressure p and the temperature T (monitored at the center with a retractable thermocouple corrected for radiation errors) are combined to obtain the molecular concentrations. Values are given in Table S1 of the Supplemental Information, along with the average residence time τ in the heated cell before photolysis. The Ar serves to slow diffusion to the cell walls and by raising the heat capacity of the mixture ensures isothermal conditions during reaction. The measured laser pulse energy E, which is corrected for window transmission, and its cross section of 0.5 cm^2 were combined with absorption

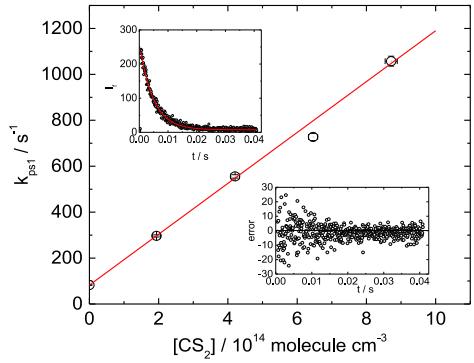

Fig. 1. Pseudo-first-order decay coefficient for H atoms as a function of CS_2 concentration. The insets show a fluorescence decay and, on an expanded scale, a plot of the residuals from the exponential fit.

cross sections of NH_3 and CS_2 of 5.0×10^{-18} and 2×10^{-16} cm^2 $molecule^{-1}$ [15,16], respectively, at 193 nm and assumed unit quantum yields to obtain estimates of the initial concentrations of [H] and [S].

Following their generation, H atoms are lost mainly through reaction (1) and via diffusion out of the observation zone, with the latter described by an effective first-order rate constant k_{diff}:

$$d[H]/dt = -k_1[H][CS_2] - k_{diff}[H] = -k_{ps1}[H] \quad (2)$$

k_{ps1} is the pseudo-first-order decay coefficient and is obtained by fitting the observed fluorescence signal to an exponential decay with time t, which does not require knowledge of the absolute [H]. At a given set of conditions (T, p, [NH_3], τ, E) variation of [CS_2] with typically 5 values from 0 to $[CS_2]_{max}$ allows determination of the second-order rate constant k_1 as the slope of a plot of k_{ps1} vs. [CS_2]. The constant k_{diff} appears in the intercept along with any minor contribution from the reaction of H with NH_3, which is slow under our conditions [17]. Linear least square fits, weighted to incorporate uncertainty in k_{ps1} and [CS_2], then yield k_1 and its 1 σ statistical uncertainty. Figure 1 shows such a linear plot, along with an example decay of time-resolved fluorescence.

3. Experimental results

Conditions and results for 42 experiments, each based on 5 determinations of k_{ps1}, are summarized in Table S1. An immediate observation is that the data are dependent on pressure. The overall range of [Ar] used was $(0.4–13) \times 10^{18}$ molecule cm^{-3}. Figure 2 shows the room temperature dependence of the second-order k_1 on [Ar], where at low [Ar] k_1 is proportional to [Ar] which is the low-pressure limiting behavior expected for the

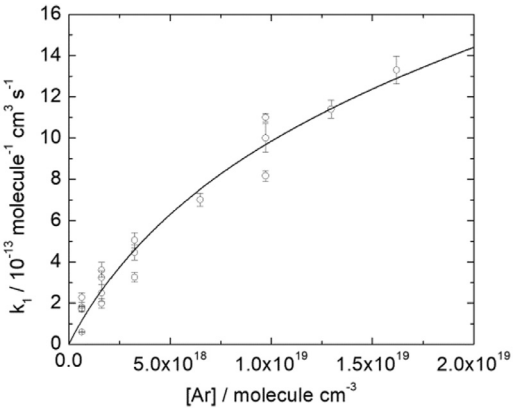

Fig. 2. Falloff curve at 295 K for $H + CS_2 + Ar$.

Table 1
Low-pressure limit data for $H + CS_2 + Ar$.

T/K	Observed $k_0/10^{-31}$ cm^6 molecule^{-2} s^{-1}	Troe fit $k_0/10^{-31}$ cm^6 molecule^{-2} s^{-1}
290	2.14 ± 0.3	2.13
350	2.80 ± 0.3	2.84
400	2.50 ± 0.3	2.52
450	1.95 ± 0.3	1.87
490	1.33 ± 0.3	1.36

Lindeman–Hinshelwood mechanism for addition to make a CS_2H species:

$$H + CS_2 \rightarrow CS_2H^* \qquad \text{rate constant } k_a \qquad (3)$$

$$CS_2H^* \rightarrow H + CS_2 \qquad \text{rate constant } k_b \qquad (4)$$

$$CS_2H^* + Ar \rightarrow CS_2H + Ar \qquad \text{rate constant } k_c \qquad (5)$$

This scheme yields

$$k_1 = \frac{k_a k_c[\mathrm{Ar}]}{k_b + k_c[\mathrm{Ar}]} = \frac{k_0 k_\infty[\mathrm{Ar}]}{k_\infty + k_0[\mathrm{Ar}]} \qquad (6)$$

where the high- and low-pressure limiting values of k_1 are $k_\infty = k_a$ and $k_0[\mathrm{Ar}] = (k_a k_c/k_b)[\mathrm{Ar}]$, respectively. For an improved treatment of the intermediate fall-off region, Troe proposed multiplying Eq. (6) by a scale factor [18] so that:

$$k_1 = \left(\frac{k_0[\mathrm{M}]}{1 + k_0[\mathrm{M}]/k_\infty}\right) \times F_{\mathrm{cent}}^{\left\{1+[\log_{10}(k_0[\mathrm{M}]/k_\infty)/(0.75-1.27\log_{10}F_{\mathrm{cent}})]^2\right\}^{-1}} \qquad (7)$$

The broadening parameter F_{cent} was set to 0.6 as recommended for an atom+linear molecule system [19]. A fit to Eq. (7) is shown as the curve on Fig. 2. The corresponding third-order k_0 is given in Table 1 and the second-order k_∞ is 5.4×10^{-12} cm^3 molecule^{-1} s^{-1}. We comment that the high-pressure extrapolation has a significant uncertainty, likely a factor of 3 or more. At higher temperatures the low-pressure region extends to higher [Ar] so that while it is possible to obtain k_0 easily the extrapolations for k_∞ are unreliable.

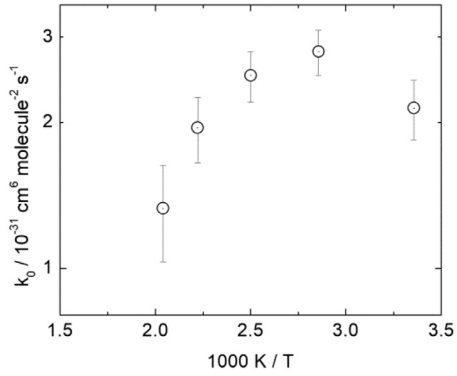

Fig. 3. Temperature dependence of the low-pressure limit for $H + CS_2 + Ar$.

The NH_3 and CS_2 concentrations and the photolysis energy were varied to change the initial radical concentrations for different rate measurements. The lack of systematic variation of the observed k_1 about the fitted fall-off curves indicates that secondary chemistry did not have a significant impact. It is likely that as an atom + atom reaction, H + S addition directly is slow, and H + CS addition may also be slow by analogy with H + CO, which assists isolation of reaction 1 from interference.

The results for the low-pressure limit are plotted in Fig. 3 and there is clear non-Arrhenius behavior, similar to that observed for example in the systems $S + C_2H_2$ [20] and $O + SO_2$ [21]. One interpretation is that the addition step (3) occurs over a modest barrier so that at low temperatures the Arrhenius behavior of k_a causes k_0 to increase with increasing temperature, while at higher temperatures the decreasing collisional energy transfer efficiency of step (5) causes k_c to decrease. An empirical summary of the data in Fig. 3, not intended for wide extrapolation outside the fitted range, is $k_0 = 7.5 \times 10^{-24}\ (T/300\ \mathrm{K})^{-14.76}$ $\exp(-5180\ \mathrm{K}/T)$ cm^6 molecule^{-2} s^{-1}.

At around 490 K a change in behavior was seen where the decays of [H] became bi-exponential. An example is shown in Fig. 4, with data also plotted on a log scale to reveal non-exponential behavior.

This means H atoms are being regenerated and a plausible reaction scheme involves decomposition of the stabilized adduct back to $H + CS_2$:

$$H + CS_2(+Ar) \rightarrow CS_2H(+Ar) \qquad \text{rate constant } k_1 \qquad (8)$$

$$CS_2H\,(+Ar) \rightarrow H + CS_2(+Ar) \qquad \text{rate constant } k_{-1} \qquad (9)$$

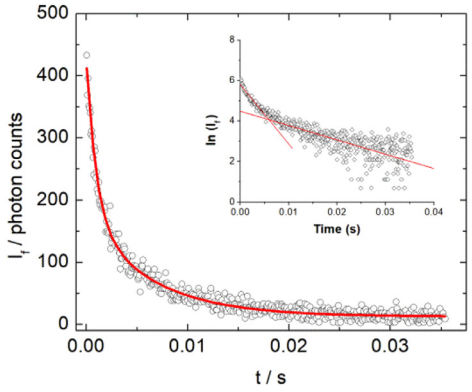

Fig. 4. Bi-exponential decay of fluorescence at 490 K. Inset with logarithmic scale.

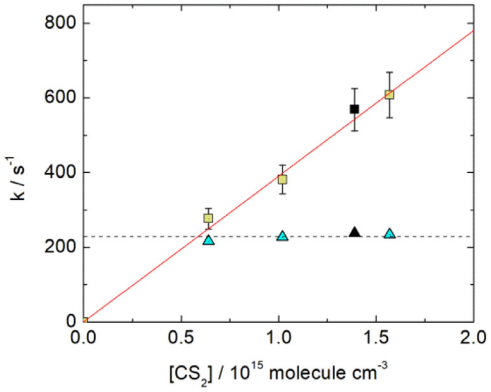

Fig. 5. Effective first-order rate coefficients vs CS_2 concentration at 490 K. Squares: addition H + CS_2. Triangles: dissociation of HSCS. Solid symbols correspond to Fig. 4.

$$\mathrm{H} \rightarrow \text{diffusion loss} \qquad \text{rate constant } k_{\mathrm{diff}} \tag{10}$$

$$\mathrm{CS_2H} \rightarrow \text{loss without H regeneration} \qquad \text{rate constant } k_{11} \tag{11}$$

The integrated biexponential rate law is [22]

$$\lambda_{1,2} = -\frac{\left(k_{\mathrm{ps1}} + k_{-1} + k_{11} + k_{\mathrm{diff}}\right) \pm \sqrt{\left(k_{\mathrm{ps1}} + k_{\mathrm{diff}} + k_{-1} + k_{11}\right)^2 - 4\left(k_{\mathrm{ps1}}k_{11} + k_{\mathrm{diff}}k_{-1} + k_{\mathrm{diff}}k_{11}\right)}}{2}$$

$$[\mathrm{H}] = [\mathrm{H}]_0 \frac{(\lambda_1 + k_{-1} + k_{11})\mathrm{e}^{\lambda_1 t} - (\lambda_2 + k_{-1} + k_{11})\mathrm{e}^{\lambda_2 t}}{\lambda_1 - \lambda_2} \tag{12}$$

The first-order parameters k_{ps1}, k_{-1} and k_{11} were varied to fit decays directly (see Fig. 4), with k_{diff} fixed by an initial experiment with no CS_2. The results are summarized in Table S2 of the Supplemental Material. One test of this rate law is that as [CS_2] is increased, k_{ps1} should increase in proportion, but the unimolecular dissociation rate constant k_{-1} should remain constant. An example is shown in Fig. 5. Although they often showed significant scatter, neither k_{-1} nor k_{11} varied consistently with [CS_2]. The loss of adduct in step (11) without hydrogen production was found to be rapid, usually faster than H-atom diffusion, suggesting some significant chemical pathway for the adduct. We speculate that a possibility is a reaction with CS_2 which is known to polymerize readily.

The forward reaction information, $k_{\mathrm{ps1}} = k_1[\mathrm{CS_2}]$, yields a further k_0 datum. The ratio k_1/k_{-1} yields the concentration equilibrium constant and hence, with transformation to unit activity at a standard state of 10^5 Pa, the dimensionless thermodynamic equilibrium constant $K_{\mathrm{eq}} = \exp(-\Delta G^0/\mathrm{RT})$. The mean ΔG^0 is -42.9 ± 2.3 kJ mol^{-1} where the uncertainty is purely statistical and represents 1 σ. Exploration of the fits to the bi-exponential decays shows that the k_{ps1}, k_{-1} and k_{11} parameters are strongly coupled, in that changes in one parameter can be largely compensated for by changes in another. The ratio k_{ps1}/k_{-1} can be reduced by a factor of 5 and the fit is still tolerable. This corresponds to a reduction of K_{eq} by a factor of 5 at 490 K, and thus an increase of ΔG^0 by 6.6 kJ mol^{-1}. To reflect this source of uncertainty the 95% confidence interval for ΔG^0 is assigned as ± 10 kJ mol^{-1}. ΔH^0 is of interest as it corresponds to minus the bond dissociation enthalpy of the CS_2H adduct, but ΔS^0 must first be established. This in part motivates the computational analysis that follows.

4. Computational analysis

Possible bound minima on the H/CS_2 potential energy surface include species where H is bonded to the C atom of CS_2 or to one of the S atoms. These possibilities were investigated by Ramesh et al. [23] who carried out calculations on HCS_2 and HSCS. These species, and connecting transition states, were characterized here using the B3LYP density functional and the cc-pV(T + d)Z basis set. The structures are provided in Table S3 of the Supplemental Material, along with vibrational frequencies scaled by a factor of 0.985. Relative enthalpies at 0 K were derived from the relative B3LYP/cc-pV(T + d)Z energies combined with the zero-point vibrational energy. Then refined

Table 2
Enthalpies at 0 K of species on the H/CS_2 potential energy surface relative to the reactants.

Species	DFT relative enthalpy/kJ mol^{-1}	W1 relative enthalpy/kJ mol^{-1}
$H + CS_2$	0	0
TS2 to HCS_2	29.9	35.5
A_1 HCS_2	−77.6	−63.3
B_2 HCS_2	−100.8	−95.1
TS1 to HSCS	1.3	4.7
cis HSCS	−66.9	−63.1
Torsion TS	−12.6	−20.4
Bend TS	−56.4	−47.4
Trans HSCS	−67.0	−65.8
TS3 to HCS_2	48.2	50.0

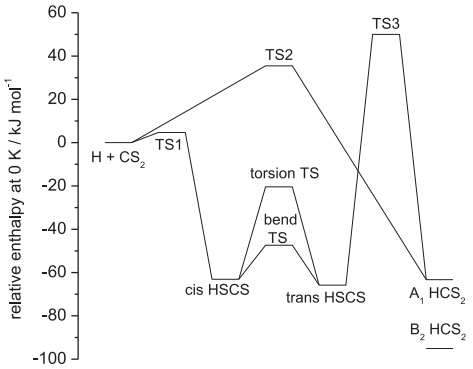

Fig. 6. Potential energy diagram for H/CS_2 based on W1 data.

energies were obtained at the same geometries by application of the W1 methodology of Martin and coworkers [24], which approximates coupled cluster theory extrapolated to the complete basis set limit, and includes corrections for scalar relativistic and core-valence electron correlation effects. These quantum calculations were carried out with the Gaussian 09 program [25].

Table 2 lists the relative enthalpies computed at the two levels of theory and permits some assessment of the reliability of the calculations. Deviations between the two methods are in the range 1–10 kJ mol^{-1}, with the exception of the A_1 state of HCS_2 where the difference is 13 kJ mol^{-1}. As in the classic example of formyloxyl (HCO_2) [26], the Hartree–Fock wavefunction is unstable with respect to symmetry-breaking away from the C_{2V} geometry, an artifact not present in density functional theory (DFT). Thus, the W1 data are somewhat suspect for this one species. Conservative error limits for the W1 enthalpies are ±10 kJ mol^{-1}.

The potential energy diagram is drawn in Fig. 6. It may be seen that H can react with CS_2 over a low barrier (TS1) to make planar *cis* and *trans* HSCS. These isomers may interconvert via SCS bending or, with greater difficulty, via rotation around the

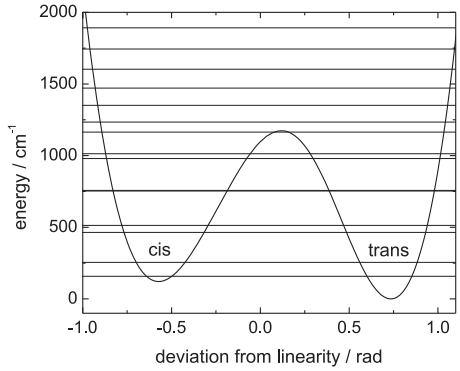

Fig. 7. Energy of HSCS as function of the SCS angle showing bent *cis* and *trans* isomers. The horizontal lines represent the corresponding eigenvalues.

central C–S bond. The significant barrier to the latter process indicates some π character in this bond. An alternative isomer is C_{2V} HCS_2 where H is bonded to the central C atom. On the basis of C_S symmetry the excited A_1 state correlates with the reactants but presumably can eventually relax to the B_2 ground state. There are significant barriers to forming HCS_2 both directly from $H + CS_2$ and by isomerization of HSCS. Thus, kinetic control favors HSCS as the product, which is consistent with the observation of this species in matrix isolation experiments by Bohn et al. [27] who co-deposited H and CS_2 with Ar at 12 K.

Having identified HSCS as the likely major product, the issue now is to deduce its entropy. A straightforward rigid rotor-harmonic oscillator treatment would miss any anharmonic effects such as those important in the entropy of chlorovinyl radicals [28]. The two HSCS isomers interconvert most easily via SCS bending. A scan along this bending mode (with all other geometry parameters allowed to optimize at a series of fixed S–C–S angles every 2°) reveals that the H–S–C angle remains locked and it is only the S–C–S angle that changes during *cis*/*trans* isomerization. The DFT energy as a function of S–C–S angle is plotted in Fig. 7 and shows an asymmetric double-well potential. The wavefunctions and corresponding eigenvalues (quantized energies) for the system were obtained using the FGH1D program [29] and they indicate strong interaction between the two minima, which therefore should not be treated as separate species at elevated temperatures.

This numerical solution of the Schrodinger equation for the 1 dimensional bending potential requires knowledge of the potential energy as a function of angle (Fig. 7) and the effective moment of inertia. The latter was derived as follows. For a linear triatomic molecule *X*–*Y*–*Z* with *X*–*Y* and *Y*–*Z* bond lengths of l_1 and l_2, Herzberg [30] notes that the bending frequency ν is related to the bending

force constant $k_\delta/(l_1 l_2)$ by

$$4\pi^2\nu^2 = \frac{1}{l_1^2 l_2^2}\left(\frac{l_1^2}{m_Z} + \frac{l_2^2}{m_X} + \frac{(l_1+l_2)^2}{m_Y}\right)k_\delta \qquad (13)$$

which is of the form $k_\delta/(l_1 l_2) \div \mu$, and the moment of inertia is $\mu\, l_1 l_2$. Because the H–S–C moiety is essential rigid, we treat the HSCS molecule like a three-particle system with $m_X = 33$, $m_Y = 12$ and $m_Z = 32$ amu. With $l_1 = 1.680$ Å and $l_2 = 1.576$ Å determined from DFT calculations, $\mu = 2.529$ amu and $\mu\, l_1 l_2 = 6.698$ amu Å^2.

The eigenvalues yield thermodynamic functions for the bending mode, assumed to be separable from the other vibrations and overall rotations that are treated using the rigid rotor-harmonic oscillator approximation. At 490 K, the bending contribution to the entropy is 16.6 J K^{-1} mol^{-1}. Had the S–C–S bending frequency in *trans* HSCS of 257 cm^{-1} been treated harmonically, its entropy would be 10.9 J K^{-1} mol^{-1}. The total entropy of HSCS is estimated to be 313.3 J K^{-1} mol^{-1}. Combined with S values for H and CS_2 [31], ΔS_{490} for $H + CS_2 \rightarrow$ HSCS is estimated as -73.8 J K^{-1} mol^{-1}. Using the experimental ΔG_{490} from the previous section, $\Delta H_{490} = -79.2$ kJ mol^{-1}. Consideration of the enthalpy corrections H_{490}–H_0 for each species then yields $\Delta H_0 = -73.2 \pm 10$ kJ mol^{-1}. This range agrees with the computed values $\Delta H_0 = -67$ (DFT) or -66 (W1) kJ mol^{-1}. Thus, it is possible to rationalize the equilibration kinetics in terms of reversible formation of HSCS. Presumably this is the product at lower temperatures too, where adduct dissociation is too slow to observe.

Consideration of TS1 yields information about the high-pressure limit for addition of H atoms to CS_2. At this transition state the SCS structure is linear (to within 0.6°) so there is no distinction between the two HSCS isomers at this early point along the reaction coordinate. Together with the W1 barrier of 4.7 kJ mol^{-1}, the standard rigid-rotor harmonic-oscillator approximations yield a transition state theory (TST) result over 290–600 K of

$$k_\infty = 1.3 \times 10^{-9} \times \exp(-7.2\,\text{kJ mol}^{-1}/\text{RT})\,\text{cm}^3\,\text{molecule}^{-1}\,\text{s}^{-1} \qquad (14)$$

The uncertainty in W1 energies proposed above implies broad uncertainties of a factor of 60 in k_∞ at 290 K, dropping to a factor of 7 at 600 K. The TST expression yields $k_\infty = 6.6 \times 10^{-11}$ cm^3 molecule^{-1} s^{-1} at 290 K, an order of magnitude larger than the fitted value of 5.4×10^{-12} cm^3 molecule^{-1} s^{-1} but within the limits proposed. Eq. (14) can be combined with the experimental determination of k_0 to make an estimate of the effective second-order rate constant for H addition to CS_2 at any pressure via Eq. (7).

At modest temperatures the likely fate of HSCS is reaction with another radical, so that CS_2 may catalyze H + radical kinetics. HSCS might also react with molecular oxygen which could open new chemical pathways. CS_2 and H both appear in kinetic models for the Claus process [2] but the only reaction considered is formation of SH + CS. The impact of the new chemistry explored here on analysis of the overall Claus process remains to be assessed by multi-reaction modeling.

5. Conclusions

Pressure-dependent kinetics have been observed for the reaction of atomic hydrogen with CS_2. At room temperature, enough of the falloff curve is available to characterize the high- and low-pressure limiting kinetics, while only low-pressure rate constants can be derived at higher temperatures. Prior matrix isolation experiments have suggested HSCS is the dominant product. At 490 K, the equilibrium $H + CS_2 \rightleftharpoons$ HSCS becomes less favorable and it is possible to characterize both addition and dissociation kinetics, and hence the equilibrium constant. Combination of this with an *ab initio* estimate of the entropy of HSCS yields a H-SCS bond dissociation enthalpy in good accord with that computed directly with W1 theory. Thus the thermochemistry and kinetics of H addition to CS_2 can now be derived over a wide range of conditions, suitable for modeling details of the Claus process for sulfur removal from sour gas.

Acknowledgments

This work was supported by the Robert A. Welch Foundation (Grant B-1174) and the National Science Foundation (Grant CBET 0756144).

Supplementary materials

Supplementary material associated with this article can be found, in the online version, at doi:10.1016/j.proci.2018.06.091.

References

[1] K. Karan, L.A. Behie, *Ind. Eng. Chem. Res.* 43 (2004) 3304–3313.
[2] I.A. Gargurevich, *Ind. Eng. Chem. Res.* 44 (2005) 7706–7729.
[3] D. Woiki, P. Roth, *Israel J. Chem.* 36 (1996) 279–283.
[4] P. Glarborg, B. Halaburt, P. Marshall, et al., *J. Phys. Chem. A* 118 (2014) 6798–6809.
[5] J.R. Petherbridge, P.W. May, D.E. Shallcross, et al., *Diamond Relat. Mater.* 12 (2003) 2178–2185.
[6] K.M. Thompson, Y. Gao, P. Marshall, et al., *J. Chem. Phys.* 147 (2017) 134302.

[7] H. Cottin, D. Despoir, *Prebiotic Evolution and Astrobiology*, in: J.T.-F. Wong, A. Lazcano (Eds.), Landes Bioscience, 2009 online.
[8] M. Mozurkewich, J.J. Lamb, S.W. Benson, *J. Phys. Chem.* 88 (1984) 6435–6441.
[9] T.L. Nguyen, B.C. Xue, R.E. Weston Jr., J.R. Barker, J.F. Stanton, *J. Phys. Chem. Lett.* 3 (2012) 1549–1553.
[10] L. Ding, P. Marshall, *J. Phys. Chem.* 96 (1992) 2197–2201.
[11] A. Goumri, D. Laakso, J.-D.R. Rocha, E. Francis, P. Marshall, *J. Phys. Chem.* 97 (1993) 5295–5297.
[12] I.M. Alecu, Y. Gao, P.-C. Hsieh, et al., *J. Phys. Chem. A* 111 (2007) 3970–3976.
[13] J. Peng, X. Hu, P. Marshall, *J. Phys. Chem. A* 103 (1999) 5307–5311.
[14] Y. Gao, N.J. DeYonker, E.C. Garrett, et al., *J. Phys. Chem. A* 113 (2009) 6955–6963.
[15] V.R. McCrary, R. Lu, D. Zakheim, et al., *J. Chem. Phys.* 83 (7) (1985) 3481–3490.
[16] G. Black, L.E. Jusinski, *Chem. Phys. Lett.* 124 (1985) 90–92.
[17] T. Ko, P. Marshall, A. Fontijn, *J Phys Chem* 94 (1990) 1401–1404.
[18] J. Troe, *J. Phys. Chem.* 83 (1979) 114.
[19] C.J. Cobos, J. Troe, *Z. Phys. Chem.* 217 (2003) 1031.
[20] S. Ayling, Y. Gao, P. Marshall, *Proc. Combust. Inst.* 35 (2015) 215–222.
[21] J. Naidoo, A. Goumri, P. Marshall, *Proc. Combust. Inst.* 30 (2005) 1219–1225.
[22] Y.V. Ayhens, J.M. Nicovich, M.L. McKee, P.H. Wine, *J Phys Chem A* 101 (1997) 9382–9390.
[23] V. Ramesh, P.H. Reddy, R. Srinivas, K. Bhanuprakash, S. Vivekanada, *Chem. Phys. Lett.* 443 (2007) 216–221.
[24] E.C. Barnes, G.A. Petersson, J.A. Montgomery Jr., M.J. Frisch, J.M.L. Martin, *J. Chem. Theory Comput.* 5 (2009) 2687–2693.
[25] M.J. Frisch, G.W. Trucks, H.B. Schlegel, et al., (Gaussian, Wallingford, CT, 2009).
[26] A.D. MacLean, B.H. Lengsfield III, J. Pacansky, Y. Ellinger, *J. Chem. Phys.* 83 (1985) 3567–3576.
[27] R.B.B. Bohn, G. Dana, L. Andrews, *J. Chem. Phys.* 96 (1992) 1582–1589.
[28] Y. Gao, I.M. Alecu, P.-C. Hsieh, et al., *Proc. Combust. Inst.* 31 (2007) 193.
[29] R. D. Johnson, III, https://www.nist.gov/mml/csd/chemical-informatics-research-group/products-and-services/fourier-grid-hamiltonian-fgh-1d (1999).
[30] G. Herzberg, *Molecular Spectra and Molecular Structure*, van Nostrand, New York, 1945.
[31] NIST-JANAF Thermochemical Tables, fourth ed, American Chemical Society American Institute of Physics, Woodbury, NY, 1998.